Pt and Ru X-ray Absorption Spectroscopy of PtRu Anode Catalysts in Operating Direct Methanol Fuel Cells

Stanislav Stoupin,[†] Eun-Hyuk Chung,[‡] Soma Chattopadhyay,[†] Carlo U. Segre,*[,†] and Eugene S. Smotkin*[,§]

Physics Division, Department of Biological, Chemical, and Physical Sciences, Illinois Institute of Technology, Chicago, Illinois 60616, Department of Chemical Engineering, Illinois Institute of Technology, Chicago Illinois 60616, and Department of Chemistry, University of Puerto Rico at Rio Piedras, San Juan, Puerto Rico 00931

Received: December 4, 2005; In Final Form: March 19, 2006

In situ X-ray absorption spectroscopy, ex situ X-ray fluorescence, and X-ray powder diffraction enabled detailed core analysis of phase segregated nanostructured PtRu anode catalysts in an operating direct methanol fuel cell (DMFC). No change in the core structures of the phase segregated catalyst was observed as the potential traversed the current onset potential of the DMFC. The methodology was exemplified using a Johnson Matthey unsupported PtRu (1:1) anode catalyst incorporated into a DMFC membrane electrode assembly. During DMFC operation the catalyst is essentially metallic with half of the Ru incorporated into a face-centered cubic (FCC) Pt alloy lattice and the remaining half in an amorphous phase. The extended X-ray absorption fine structure (EXAFS) analysis suggests that the FCC lattice is not fully disordered. The EXAFS indicates that the Ru−O bond lengths were significantly shorter than those reported for Ru−O of ruthenium oxides, suggesting that the phases in which the Ru resides in the catalysts are not similar to oxides.

Introduction

Since the introduction of PtRu 38 years ago,[1] the optimum component mole fractions, preparative method, and the link between compositions suggested by surface science studies[2−5] and compositions empirically optimized (e.g., Johnson Matthey (JM) PtRu (1:1 black)) remain unresolved. The face-centered cubic (FCC) lattice parameters of Pt-based nanostructured binary and ternary catalysts typically exceed those of Vegard law-abiding[6] arc-melted alloys of the same overall composition, suggesting incomplete incorporation of the smaller Ru atoms into the FCC Pt alloy phase, with the ghost Ru hidden in an amorphous phase.[7−9] The X-ray diffraction (XRD) pattern of as-received JM PtRu (1:1) showed only disordered FCC reflections with a 3.883 Å lattice parameter, corresponding to an alloy phase composition of PtRu (65:35).[10] The overall composition, determined by X-ray fluorescence (XRF), is PtRu (1.04:1). Taken together, this suggests a PtRu (65:35) FCC lattice intimate with ghost Ru residing in an amorphous phase-(s).

Elucidation of nanostructure−function relationships is elusive when the catalyst nanostructure is highly reflective of environmental conditions; X-ray absorption near edge structure (XANES) spectroscopy of carbon-supported PtRu in membrane electrode assemblies (MEAs) of H_2/air fuel cells, prior to fuel cell assembly, during fuel cell operation, and ex situ after fuel cell use,[11] confirm that Pt and Ru of the as-received PtRu are highly oxidized, during H_2/air fuel cell operation the PtRu is rapidly reduced to a nearly metallic state, and after fuel cell operation and removal of the MEA from the fuel cell, the PtRu is reoxidized, although to lesser extent than the as-received catalyst. Thus structure−function elucidation requires that analytical techniques be applied in appropriate catalyst environments.

X-ray absorption spectroscopy (XAS) has been previously used to study direct methanol fuel cell (DMFC) electrocatalysts;[12−18] however this report differs from prior studies in that Ru and Pt extended X-ray absorption fine structure (EXAFS) and XANES were obtained in transmission mode through purely conventional liquid feed DMFC, as the potential was scanned through the current onset potential. The Ru and Pt EXAFS were simultaneously fit to characterize the bulk structure of phase segregated nanostructured unsupported PtRu.

The XAS data were augmented with ex situ XRD and XRF analysis to elucidate the operational catalyst structure during fuel cell operation.

Experimental Section

Electrode Preparation. Unsupported anode catalyst ink dispersions were prepared by an adaptation of Wilson's method[19] where the ink was painted directly onto the gas diffusion backings.[20] The JM PtRu 1:1 (Johnson Matthey, stock no. 41171, lot no. C13K06) is mixed with 5 wt % Nafion (Aldrich) and water followed by gentle stirring for 3 days. To ensure that the Pt spectra measured were solely attributable to the anode catalyst, the cathode ink was prepared by mixing Pd (30 wt % on activated carbon, Aldrich) with 5 wt % Nafion followed by stirring for 3 days. The anode and cathode inks were painted onto carbon paper (TGPH-060, 0.17 mm thickness, Plain) and carbon cloth (E-TEK, ELAT/NC/DS/V2 double sided ELAT electrode, 20% wet proofed), respectively. The carbon fabrics are used as electrode diffusion backings. The macropores of the diffusion backings were blocked with high-surface-area carbon to prevent deep penetration of the catalyst into the

* Authors to whom correspondence should be addressed. E-mail: segre@iit.edu; esmotkin@cnnet.upr.edu.
[†] Department of Biological, Chemical, and Physical Sciences, Illinois Institute of Technology.
[‡] Department of Chemical Engineering, Illinois Institute of Technology.
[§] Department of Chemistry, University of Puerto Rico at Rio Piedras.

10.1021/jp057047x CCC: $33.50
Published on Web 04/29/2006

backing thus optimizing the catalyst utilization. The painted diffusion backings (electrodes) were dried in an oven (120 °C) and weighed. The paint and bake process was repeated until a metal loading of 4.0 mg/cm^2 was attained. A Nafion 117 (DuPont) membrane was hot pressed between the anode and cathode catalyzed diffusion backings to yield the MEA. The MEAs were conditioned by a flow of Nanopure water at the anode side for 2 days prior to obtaining Pt L_{III}-edge and Ru K-edge data at the Advanced Photon Source (APS), Argonne, IL.

The catalyst utilization of the MEAs prepared by the method of this study was measured by Gurau.[20] CO stripping experiments were performed to determine the electrocatalytically active area corresponding to the geometric area of the MEA electrode as previously described. The Brunauer−Emmett−Teller (BET) surface area of the catalyst was 80.6 m^2/g, and the typical catalyst loading in a 5.0 cm^2 MEA anode is 0.013 g Pt. Thus the sum total of the BET area of the catalyst incorporated into the MEA (A_{BET}) was 1.0 m^2. After adsorption of CO on the anode side of the MEA, two successive scans were obtained. The first scan removed the adsorbed CO. The second scan was used as a baseline for integration of the CO stripping peak. The electrochemically active area of the MEA electrode (A_{act}) is calculated as follows

$$A_{act} = Q_{meas}/Q_{mono}$$

The integral of the stripping wave (volts × amps) divided by the scan rate (0.005 V/s) is Q_{meas} and has dimensions of Coulombs. The charge required to oxidize a monolayer of linearly adsorbed CO on Pt is Q_{mono} (~4 C/m^2).[21] The mean value of the calculated A_{act} was 0.84 m^2. Gurau defined the fraction of the BET surface area utilized as the ratio of A_{act} to A_{BET}. A_{act}/A_{BET} is 80%.

In Situ XAFS Fuel Cell Experimental Setup. The in situ synchrotron EXAFS fuel cell has been described in detail.[11,22] A mass flow controller (model FC-260, Tylan Corporation, Torrance, CA) was used to deliver H_2 (4% balanced N_2 at 100 mL/min) to the counter electrode, enabling its use as a dynamic hydrogen electrode (DHE) reference for acquisition of anode polarization curves. A high-precision computerized syringe pump (ISCO, Inc., model 100DX, Lincoln, NE) was used to deliver aqueous methanol. A back-pressure of 120 Torr was applied to the anode to prevent CO_2 phaseout during methanol oxidation. An AutoLab potentiostat (PGSTAT20, EcoChemie, Netherlands) was used to measure anode polarization curves and for potential control during EXAFS and XANES experiments. All fuel cell data were obtained at 35 °C with 0 psig at the cathode. DMFC polarization curves were obtained with air at the cathode, while anode polarization curves were obtained using the counter electrode as a DHE.

The in situ fuel cell XAS data were acquired at the Materials Research Collaborative Access Team (MRCAT) beamline, Sector 10-ID, of the Advanced Photon Source at Argonne National Laboratory, IL. All in situ XAS data were obtained in transmission mode with a Pt foil or Ru powder sample used as reference standards. The 30-cm-long incident and transmitted beam ionization chambers were both operated with flowing N_2 for the Pt L_{III}-edge and N_2 and 80% N_2/ 20% Ar (incident/transmitted) for the Ru K-edge. A flat ULE glass mirror with a Rh stripe and a Pt stripe (for measurement at the Pt L_{III}- and Ru K-edges, respectively) was used for harmonic rejection. The unsupported catalyst in the fuel cell gave absorption edge jumps of $\Delta\mu x = 0.05$ for Ru and $\Delta\mu x = 0.17$ for Pt.

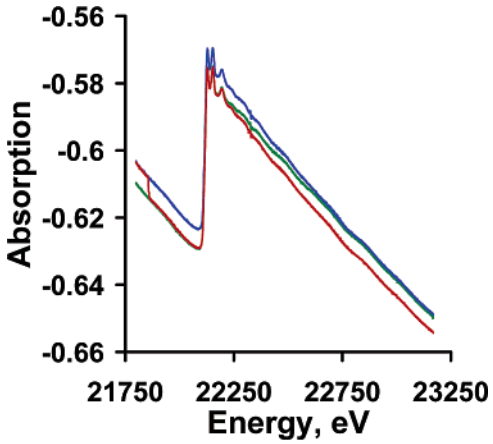

Figure 1. Absorption transition events.

Multiple quick scans were taken at the Pt L_{III}- (11 564 eV) and Ru K-edges (22 117 eV) at applied potentials (vs DHE) of 250, 300, 350, 400, 450, 500, and 550 mV with 0.1 and 2 M methanol and water on the anode side and 4% dry H_2 balanced N_2 at the cathode side. Reference XANES and EXAFS spectra at Ru K- and Pt L_{III}-edges were measured at room temperature on Pt foil (EXAFS Materials, Inc., Danville, CA), Pt black, Ru powder (Alfa Aesar, Ward Hill, MA), RuO_2 (Alfa Aesar, Ward Hill, MA), $RuO_2{\cdot}H_2O$ (Alfa Aesar, Ward Hill, MA), and as-received PtRu catalyst (JM 1:1 black). All of the reference materials except for the Pt foil were ground to a fine powder and dusted onto scotch tape. Sufficient layers of tape were used to obtain $\Delta\mu x \approx 1$ at each absorption edge for the reference spectra.

Multiple scans obtained for each experimental condition were rebinned, summed, deglitched, and normalized using Athena.[23] Athena employs the AUTOBK algorithm for background minimization below the R_{bkg} value, which in our case was set to 1.0.

Data were modeled using Artemis with theoretical standards calculated by FEFF6.[23,24] The fits were performed simultaneously using k, k^2, and k^3 weighting and included background refinement. The analysis was limited to first-shell, single-scattering paths generated using Pt and Ru atoms arranged in a Pt-like FCC structure and Pt−O and Ru−O paths, when necessary, taken from the respective oxide structures. The EXAFS amplitude for each scattering path was parametrized as the product of the coordination number and a passive electron reduction factor. We obtained values for the Pt−Pt, Pt−Ru, Ru−Pt, and Ru−Ru (absorber−scatterer) coordination numbers by fixing the passive electron reduction factors for both Pt and Ru to 0.81 as reported by Nashner et al.[25]

Results

Figure 1 shows absorption transition events that are often present in the raw data. These events could be attributed to the creation of a CO_2 bubble in the fuel cell flow field (red line) at 21 870 eV concomitant with a reduction in absorption followed by the gradual expulsion of the bubble from 22 200 to about 22 750 eV (green line) resulting in an increase in absorption. Such density fluctuations within the area exposed to the X-ray beam reduce the amount of EXAFS data available for signal averaging. This phenomenon was minimized by operation of the fuel cell at 35 °C (relevant to palm power) and application of a back-pressure (120 Torr) to the anode outlet to prevent the phaseout of CO_2 from the methanol fuel stream.

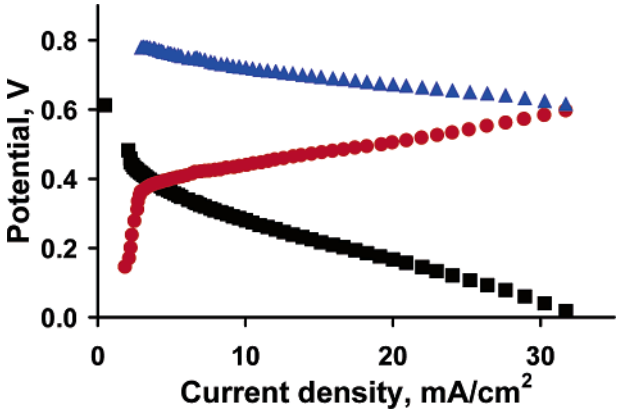

Figure 2. Anode polarization: 0.1 M MeOH versus 4% H_2 balanced N_2 at the counter electrode (red). Full cell polarization (35 °C): MeOH (0.1 M, 1 mL/min)/air (100 sccm) (black). Calculated cathode polarization: (full cell + anode curve) (blue).

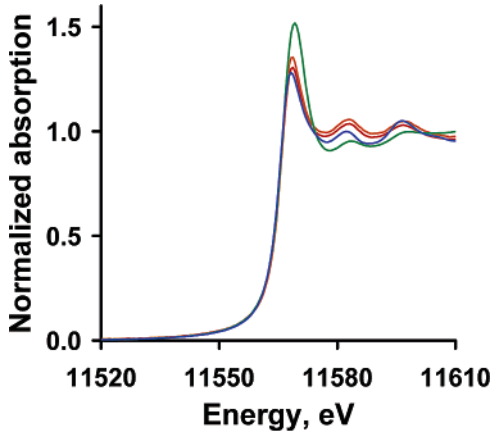

Figure 3. Pt L_{III}-edge XANES: In situ catalyst at 450 mV (red), in situ catalyst at 450 mV from another run (orange), Pt foil (blue), and as-received catalyst (green).

Figure 2 shows the anode (red), full cell (black), and calculated cathode (blue) polarization curves for a 35 °C DMFC. The current onset at 380 mV vs Pd/H_2 was the basis for selection of the potential range for the XAS (250−450 mV) bracketing the current onset potential. Although the consensus is that water activation is the methanol oxidation rate-limiting step, the nature of the activated species (e.g., Ru·H_2O, Ru−OH, Ru═O, etc.) is somewhat speculative.

Figure 3 shows the Pt L_{III}-edge data; the red line shows Pt XANES at 450 mV obtained in DMFC mode, while the green and blue lines are the as-received catalyst (mounted on scotch tape) and Pt foil XANES respectively, also measured in transmission. The increased white line intensity of the alloyed Pt (red) versus the pure Pt (blue) is due to alloy-induced d-band vacancies, as was observed in XANES from an arc-melted $Pt_{80}Ru_{20}$ alloy.[11] The large edge intensity of the green curve signifies extensive oxidation of the as-received catalyst. Although the potential-dependent (250, 300, 350, 400, and 450 mV) EXAFS (Figure 4) are color-coded, the near perfect overlap confirms that, within the operating potential window, the Pt is insensitive to potential, similarly to the Pt within supported PtRu catalyst in a H_2/air fuel cell.[11] Figure 5 shows the excellent first-shell fit of the 350 mV EXAFS data (blue) with a model fit (red) simulating a totally metallic environment (fit range 1.5 to 3.1 Å) of mixed Pt and Ru atoms.

Figure 6 shows the ex situ Ru K-edge XANES of metallic Ru powder (blue), in situ catalyst Ru at 350 mV (red), as-received PtRu (1:1) catalyst (green), Ru oxide (black), and

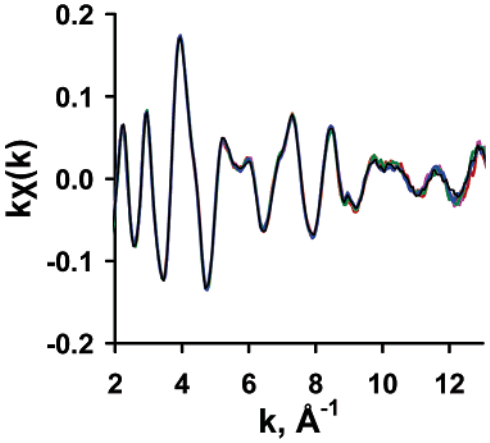

Figure 4. Potential-dependent Pt L_{III}-edge EXAFS in *k*-space at 0.1 M MeOH, color-coded for anode potential (250, 300, 350, 400, and 450 mV).

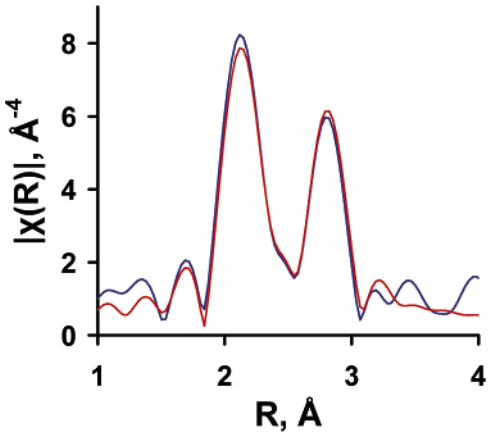

Figure 5. Pt EXAFS fit (red line) to in situ catalyst data at 450 mV (blue) as a totally metallic environment (only Pt and Ru nearest neighbors). Fit range is from 1.5 to 3.1 Å.

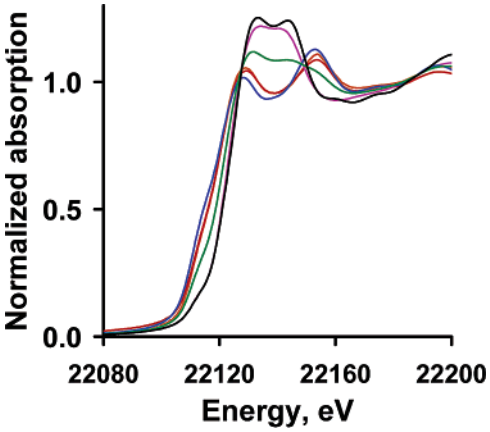

Figure 6. Ru K-edge XANES: Operating fuel cell anode at 450 mV (red and orange—another similar experiment), metallic Ru powder (blue), Ru oxide hydrate, (pink), Ru oxide (black), and as-received JM PtRu (1:1) (green) standards mounted on scotch tape.

Ru oxide hydrate (pink). The coincidence of the catalyst Ru edge at 350 mV (red) with the metallic Ru powder (blue) confirms that within the DMFC operating potential window the Ru component is primarily metallic. The deviation of the red from the blue line at 22 120 eV reflects the difference between the nearest-neighbor environments of pure Ru (hexagonal) and Ru in a PtRu catalyst (FCC). The as-received catalyst edge (green) is intermediate in energy between the metallic (blue and

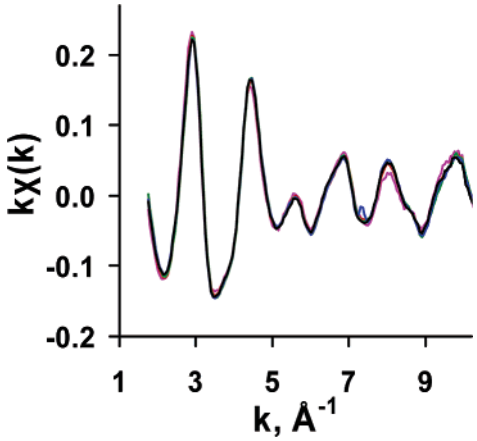

Figure 7. Potential-dependent Ru K-edge EXAFS in *k*-space at 0.1 M MeOH, color-coded for anode potential (250, 300, 350, 400, and 450 mV).

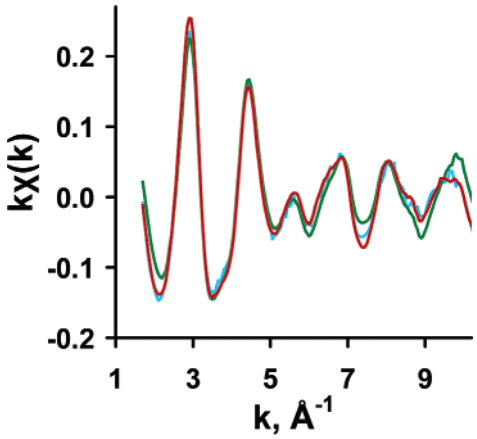

Figure 8. Ru K-edge EXAFS in *k*-space at (350 mV) in H_2O (blue) and 0.1 M MeOH (green) and 2 M MeOH (red).

red) lines and the oxides of Ru (pink and black) confirming that the as-received catalyst is substantially oxidized. The near edge data of the as-received catalyst is intermediate between the saddle point of the Ru oxide and the metallic catalyst line (red), again confirming a substantially oxidized as-received catalyst.

The potential-dependent EXAFS spectra in *k*-space (Figure 7) do not support a potential-controlled core structure transition over the entire range of 250−450 mV. Moreover the overall Ru nearest-neighbor environment (includes core and surface) shows no potential dependence within the DMFC operating potential window.

Figure 8 shows the fuel cell EXAFS *k*-space spectra (350 mV) in H_2O (blue) and 0.1 M (green) and 2 M MeOH (red). The order in which the experiments were conducted were 0.1 M MeOH, 2 M MeOH, and finally water.

Figures 7 and 8 taken together suggest that the Ru (within the nanocrystallite, ghost phase and surface Ru taken together) nearest-neighbor environment is invariant within the DMFC potential window and, within the experimental error, not affected by variations of concentration from 0 to 2 M MeOH. Viswanantan showed that after reduction of the anode catalyst in a fuel cell anode environment removal of the membrane electrode assembly and exposure to air resulted in only partial oxidation of the catalyst. The catalyst remained primarily metallic.[11] The XANES data are more suitable for quantitative analysis of oxidation states. Later we will show that within experimental

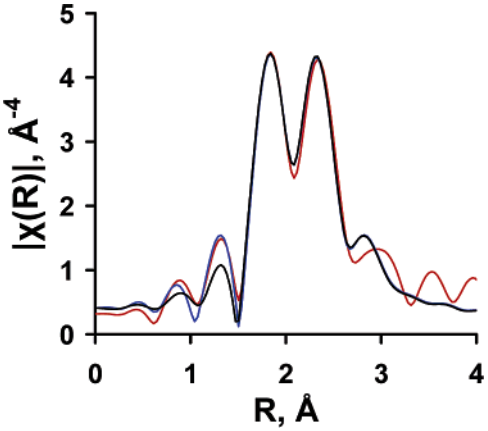

Figure 9. Fourier-transformed Ru EXAFS (magnitude) at 450 mV (red), fit as fully metallic (only Ru and Pt nearest neighbors) (black), as a metallic environment with O nearest neighbors (blue). The peak at 1.3 Å is due to oxygen nearest neighbors. Fit range is from 1 to 3.1 Å.

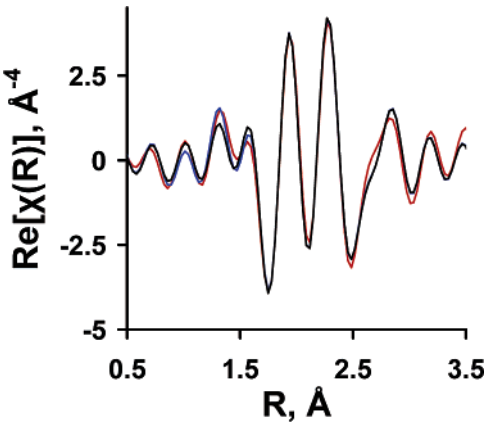

Figure 10. Real part of $\chi(R)$: Ru EXAFS at 450 mV (red), fit as fully metallic (only Ru and Pt nearest neighbors) (black), as a metallic environment with O nearest neighbors (blue).

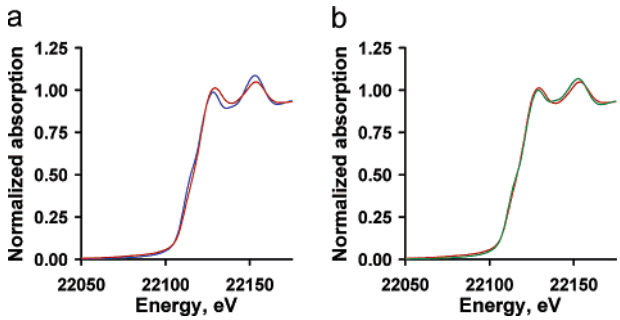

Figure 11. Ru K-edge least-squares fit at 350 mV: (a) 0.1 M MeOH XANES (red) with only Ru ($\chi = 1.28$) (blue); (b) RuO_2 hydrate and Ru metal ($\chi = 0.45$).

error of the XANES data the level of oxidation of the core structure of the catalyst is the same in water or in 2 M methanol (Figure 12).

Figure 9 shows Ru EXAFS (red) obtained during fuel cell operation. The black line is the EXAFS fit as a fully metallic (only Ru and Pt nearest neighbors) environment. The addition of a Ru−O path and associated Debye−Waller factor gives a substantially better EXAFS fit. Figure 10 shows the real part of $\chi(R)$ with a peak at 1.3 Å due to oxygen nearest neighbors (fit range 1 to 3.1 Å).

Figure 11 shows an example Ru XANES edge least-squares fit using Ru metal and Ru oxide hydrate as reference materials.

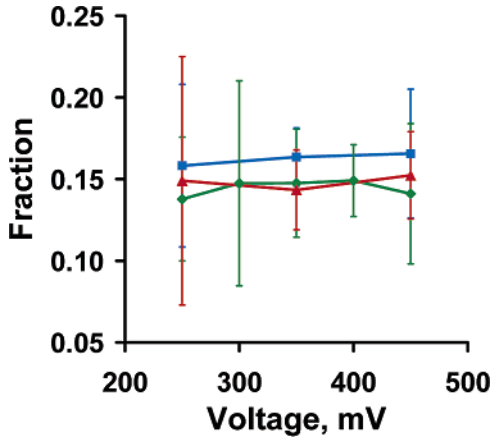

Figure 12. Least-squares fits of in situ XANES with Ru powder and Ru oxide hydrate standards showing fractions of Ru oxide hydrate versus potential in pure H_2O (blue), 0.1 M MeOH (green), and 2 M MeOH (red).

The fit with only a Ru metal component is plotted in Figure 11a while Figure 11b shows the fit using both references. The fit using the two reference spectra is superior both visually and statistically (using χ^2 as the measure of goodness of fit).

Strictly speaking, a fit with the above two standards would be appropriate for a system that is a mixture of two phases: metallic Ru and Ru oxide hydrate. The Ru oxide hydrate is probably not the most appropriate fit for chemisorbed oxygen on metallic Ru surfaces where the core Ru has Ru nearest neighbors in the first shell. The least-squares fits of the in situ XANES with Ru powder and Ru oxide hydrate standards (Figure 12) show that the fractions of Ru oxide hydrate required for the best fit in pure H_2O and 0.1 and 2 M methanol is, within experimental error, invariant within a potential window that brackets the onset potential. The pure water data shows the most oxide, as expected. The precision of the extent of oxide fit is very good when considering the overall state of oxidation of the Ru in the catalyst. Unfortunately the least-squares data cannot be used to make a statement about changes in the extent of oxidation of surface Ru because there is no way to know the distribution of the Ru−O bonds between the bulk and the surface. If a substantial amount of the Ru−O bonds are in a stable phase, then observation of the effect of potential on the number of nearest-neighbor oxygens to Ru on the surface would involve a change that is small with respect to the total number of Ru−O bonds. Nevertheless, the data clearly show that there is no change in the core structure of the catalyst throughout the DMFC potential window and the core is essentially metallic. The important finding is that the fraction of oxide required for the fit is very low, suggesting that the majority of the Ru in the catalyst is in a metallic state. The distribution of Ru−O bonds between the bulk and the surface cannot be addressed with these data.

The EXAFS structural parameters obtained from the fit are summarized in Table 1. The results of two independent EXAFS experiments, on two MEAs, are presented (MEA1 and MEA2).

The MEA1 data were taken at different anode potentials in 0.1 M methanol. The invariance of the Ru and Pt EXAFS within the potential widow studied justifies the simultaneous fitting of the 0.1 M Pt and Ru EXAFS. Therefore, a multiple dataset fit (i.e., data at all potentials fit simultaneously) was performed to obtain the fit values of the MEA1 column of Table 1.

The results from the multiple dataset fit were confirmed by repeating the experiment with a second electrode (MEA2) prepared identically to MEA1 and studied at an anode potential of 450 mV. During the MEA2 experiment particular care was taken to minimize background contributions that were the cause of the observed negative Debye−Waller factor for the Ru−O path in the MEA1 data. The structural parameters obtained from MEA2 are in remarkable agreement with the MEA1 parameters with the exception of Ru−O Debye−Waller factor, which was positive for MEA2.

The ratio of the atomic fractions ratio $y_{Ru} = N^{Ru}{}_{Pt}/N^{tot}$ (fraction of Ru atoms around Pt), and similarly y_{Pt} (fraction of Pt atoms around Ru) where N^{tot} is the fitted total number of nearest neighbors, can be used to obtain the ratio of Ru to Pt in the FCC lattice. That ratio, 0.49, is remarkably close to the 0.52 value obtained from the lattice parameter analysis. The fit value of $y_{Ru} = 0.27 \pm 0.02$ (less than the Ru composition in the FCC phase, 0.34) suggests that the EXAFS model of the FCC lattice requires some segregation of one of the components rather than a perfectly random arrangement. The first-shell coordination number (N^{tot}) of 8.2 is consistent with previously reported values

TABLE 1: Catalyst Structural Parameters from Pt and Ru EXAFS for Three Different Samples[a]

EXAFS parameter	notation	MEA1	MEA2	as-received catalyst
Ru around Pt fraction[b]	y_{Ru}	0.27(0.02)	0.30(0.07)	0.25(0.07)
Pt around Ru fraction	y_{Pt}	0.55(0.02)	0.49(0.06)	0.57(0.07)
Ru−Ru bond DWF[c] (Å^2)	σ^2_{Ru-Ru}	0.0037(0.0005)	0.0045(0.0012)	0.0042(0.0018)
Ru−Pt bond DWF (Å^2)	σ^2_{Ru-Pt}	0.0038(0.0005)	0.0034(0.0014)	0.0038(0.0018)
Pt−Pt bond DWF (Å^2)	σ^2_{Pt-Pt}	0.0057(0.0003)	0.0047(0.0009)	0.0064(0.0011)
Ru−Ru bond length (Å)	R_{Ru-Ru}	2.649(0.003)	2.652(0.007)	2.66(0.01)
Ru−Pt bond length (Å)	R_{Pt-Ru}	2.698(0.003)	2.695(0.009)	2.70(0.01)
Pt−Pt bond length (Å)	R_{Pt-Pt}	2.717(0.003)	2.716(0.010)	2.71(0.01)
total number of first-shell atoms	N^{tot}	8.2(0.2)	8.2(0.7)	5.5(1.1)
Ru−O bond DWF (Å^2)	σ^2_{Ru-O}	−0.003(0.004)	0.01[d]	0.0057(0.0024)
Ru−O bond length (Å)	R_{Ru-O}	1.86(0.02)	1.88(0.05)	1.94(0.03)
Ru−O coordination number	N_{Ru-O}	0.3(0.1)	0.4(0.2)	2.6(0.6)
Pt−O bond DWF (Å^2)	σ^2_{Pt-O}	n/a	n/a	0.0049(0.0023)
Pt−O bond length (Å)	R_{Pt-O}	n/a	n/a	1.93(0.03)
Pt−O coordination number	N_{Pt-O}	n/a	n/a	1.5(0.4)

[a] MEA1 is in 0.1 M methanol with all potentials fit simultaneously. MEA2 is in 0.1 M methanol at 450 mV anode potential (improved EXAFS background, similarly prepared MEA), and the as-received catalyst (same structural model plus Pt−O bond) is also given. The uncertainties are given in parentheses. [b] Fractional coordination numbers are defined as follows: $y_{Ru} = N^{Ru}{}_{Pt}/N^{tot}{}_{Pt}$ and $y_{Pt} = N^{Pt}{}_{Ru}/N^{tot}{}_{Ru}$ where $N^{Ru}{}_{Pt}$ is the average number of Ru neighbors around a Pt atom and $N^{Pt}{}_{Ru}$ is the average number of Pt neighbors around a Ru atom. $N^{tot}{}_{Ru} = N^{tot}{}_{Pt} = N^{tot} -$ (total number of FCC first-shell atoms). By definition: $N^{tot}{}_{Ru} = N^{Ru}{}_{Ru} + N^{Pt}{}_{Ru}$ and $N^{tot}{}_{Pt} = N^{Pt}{}_{Pt} + N^{Ru}{}_{Pt}$. These relationships enable derivation of coordination numbers for each pair of atoms using the above fitted parameters: $N^{Ru}{}_{Ru} = N^{tot}(1 - y_{Pt})$, $N^{Pt}{}_{Ru} = N^{tot}y_{Pt}$, $N^{Pt}{}_{Pt} = N^{tot}(1 - y_{Ru})$, $N^{Ru}{}_{Pt} = N^{tot}y_{Ru}$. [c] Debye−Waller factor. [d] Fixed parameter in the fit.

for EXAFS of high-surface-area PtRu. Bond lengths and Debye−Waller factors are consistent with available EXAFS literature values for Pt−Ru catalyst.

The 1.87 Å Ru−O bond length obtained in this study was very reproducible from MEA1 to MEA2 and shorter than the 2.02 Å reported for RuO_2 or $RuO_2 \cdot H_2O$.[26] This is not unexpected as our analysis shows that the Ru is primarily metallic in the Johnson Matthey catalyst during fuel cell operation. In samples with 2.02 Å Ru−O distances there are no Ru−Ru bonds. This is very different from Ru incorporated in either an FCC PtRu lattice or a primarily metallic amorphous Ru phase. Examination of Table 1 suggests that the 1.87 Å value is part of a systematic trend. The Ru−O distance in the as-received catalyst is 1.94 Å, much closer to the 2.02 Å reported in other studies. Our XANES data shows that the as-received catalyst is highly oxidized. The as-received catalyst can be fit with a similar model yielding an overall metal coordination number (N^{tot}) of 5.5 and significantly larger number of Ru−O (2.6) and Pt−O (1.5) bonds averaged over all atoms in the catalyst (Table 1). The XANES also shows that upon introduction of the reducing fuel the catalyst is reduced to an essentially metallic state. This is indicative of a structural transformation from an as-received catalyst where oxygen penetrates deep into the FCC nanoparticles (and the ghost phase) to an operational catalyst that is metallic with a small amount of residual oxygen either at the surface of the clusters or in the ghost phase. The trend is thus 2.02 Å for Ru−O bonds in fully oxidized Ru, 1.94 Å for Ru−O lengths in substantially oxidized Ru (within the as-received catalyst), and 1.87 Å for Ru−O bonds in the nanostructured catalyst, which is not similar to a fully oxidized phase. While it is true that the Ru−O EXAFS parameters are correlated with the EXAFS background in our fits because of overlap of the weak scattering from the O nearest neighbors with the structureless part of the absorption coefficient in the low *R* region around 1.5 Å, the reproducibility of the Ru−O distances that we obtain with two independent MEAs coupled with a systematic trend in the Ru−O distances with the extent of oxidation suggest that the low value that we obtain for the operational catalyst must be taken seriously.

An average cluster size of 3.6 nm leads to an expected average number of metal−metal bonds of about 10.8 as opposed to 12 for bulk FCC.[27] The N^{tot} values obtained here, 8.2 and 5.5 for the catalyst in the fuel cell and the as-received catalyst, respectively, are significantly lower than expected for these nanoparticles and hint that the removal of oxygen from the catalyst may not be accompanied by a complete restructuring of the metal atoms to a close-packed structure, leading to an enhanced surface area which could be important for the proper functioning of the catalyst. The spectroscopy data, in combination with XRD and X-ray fluorescence data, yield a model for the JM PtRu (1:1) catalyst that includes an FCC lattice of PtRu of 65% Pt and phased out Ru that is primarily metallic. The average oxidation state of the Ru is not a function of potential or methanol concentration (within the studied potential window) and corresponds to no more than 30% oxidation of the phased out Ru, or somewhat less than one O nearest neighbor per Ru.

Conclusions

The first-shell modeling of EXAFS data from nanostructured PtRu catalysts demonstrates that data obtained under actual reaction conditions is required for combined analysis with ex situ XRD and XRF data because substantial differences in oxidation states of catalyst components are typical in as-received catalysts versus operational catalysts. Gasteiger reported ∼10% Ru as optimum at room temperature and an increase in Ru with increasing temperature (33% at 60 °C) on arc-melted Pt alloy surfaces.[3] The gap between predictions based on model surface studies and the fact that PtRu (∼1:1) is the most commercialized high-surface-area DMFC catalyst diminishes with the knowledge that the alloy phase of the nanostructured catalyst is substantially richer in Pt because of Ru phaseout. This is the first work, to our knowledge, where Ru and Pt EXAFS data were fit simultaneously to characterize the bulk structure of a nanostructured catalyst with results that are consistent with previous lattice parameter analysis of the same catalyst. We demonstrate that XAS can be used for quantitative analysis of the bulk structure.

The least-squares fit of the XANES shows that there is at best minimal change in the overall state of oxidation of the catalyst Ru at the current onset potential of 380 mV. Recently Tolmachev reported an elegant study of surface XAS of Ru decorated onto the surface Pt particles.[28] Our goal is to improve the sensitivity of our method to enable the acquisition of surface-sensitive data on real-world nanocatalysts that have substantial subsurface Ru[29] as is the case with state-of-the-art DMFC catalysts today. To that end we are modifying the cell for fluorescent studies.

Acknowledgment. MRCAT operations are supported by the Department of Energy and the MRCAT member institutions. The APS is funded by the U. S. Department of Energy, Office of Science, Office of Basic Energy Sciences under Contract No. W-31-109-Eng-38. This work was supported by the Army Research Office HSI Grant No. W911NF-05-1-0020 and the NASA-UPR Center for Nanoscale Materials Grant No. NCC3-1034.

References and Notes

(1) Niedrach, L. W.; McKee, D. W.; Paynter, J.; Danzig, I. F. *Electrochem. Technol.* **1967**, *5*, 318.
(2) Kim, H.; Rabelo de Moraes, I.; Tremiliosi-Filho, G.; Haasch, R.; Wieckowski, A. *Surf. Sci.* **2001**, *L203*−*L212*, 474.
(3) Gasteiger, H. A.; Markovic, N. M.; Ross, P. N., Jr.; Cairns E. J. *J. Electrochem. Soc.* **1994**, *141*, 1795−1803.
(4) Chrzanowski, W.; Wieckowski, A *Langmuir* **1998**, *14*, 1967.
(5) Rhee, C. K.; Wakisaka, M.; Tolmachev, Y. V.; Johnston, C. M.; Haasch, R.; Attenkofer, K.; Lu, G. Q.; You, H.; Wieckowski, A. *J. Electroanal. Chem.* **2003**, *554*−*555*, 367−378.
(6) Cullity, B. D. *Elements of X-ray Diffraction*, 2nd ed.; Addison-Wesley: Reading, MA, 1978; p 376.
(7) Ley, K. L.; Liu, R.; Pu, C.; Fan, Q.; Leyarovska, N.; Segre, C.; Smotkin, E. S. *J. Electrochem. Soc.* **1997**, *144*, 1543−49.
(8) Gurau, B.; Viswananthan, R.; Liu, R.; Lafrenz, T. J.; Ley, K. L.; Smotkin, E. S. *J. Phys. Chem. B* **1998**, *102*, 9997−10003.
(9) Rolison, D. R.; Hagans, P. L.; Swider, K. E.; Long, J. W. *Langmuir* **1999**, *15*, 774−779.
(10) Smotkin E. S.; Diaz-Morales, R. R. New Electrocatalysts by Combinatorial Methods. *Annu. Rev. Mater. Res.* **2003**, *33*, 557−579.
(11) Viswanathan, R.; Hou, G.; Liu, R.; Bare, S. R.; Modica, F.; Mickelson, G.; Segre, C. U.; Leyarovska, N.; Smotkin, E. S. *J. Phys. Chem. B* **2002**, *106*, 3458−3465.
(12) Lampitt, R. A.; Carrette, Linda P. L.; Hogarth, M. P.; Russell, A. E. *J. Electroanal. Chemistry* **1998**, *460*, 80−87.
(13) Russell, A. E.; Maniguet, S.; Mathew, R. J.; Yao, J.; Roberts, M. A.; Thompsett, D. *J. Power Sources* **2001**, *96*, 226−232.
(14) Mukerjee, S.; McBreen, J. *J. Electroanal. Chem.* **1996**, *448*, 163−171.
(15) O'Grady, W. E.; Hagans, P. L.; Pandya, K. I.; Maricle, D. L. *Langmuir* **2001**, *17*, 3047.
(16) Bae, I. T.; Scherson, D. A. *J. Electrochem. Soc.* **1998**, *145*, 80.
(17) Holstein, W. L.; Rosenfeld, H. D. *J. Phys. Chem. B* **2005**, *109*, 2176−2186.
(18) Mukerjee, S.; Urian, R. C. *Electrochim. Acta* **2002**, *47*, 3219−3231.
(19) Wilson, M. S.; Gottesfeld, S. *J. Appl. Electrochem.* **1992**, *22*, 1−7.
(20) Gurau, B.; Smotkin, E. S. *J. Power Sources* **2002**, *112*, 339−352.

(21) Dinh, H. N.; Ren, X.; Garzon, F. H.; Zelenay, P.; Gottesfeld, S. *J. Electroanal. Chem.* **2000**, *491*, 222.
(22) Viswanathan, R.; Liu, R.; Smotkin, E. S. *Rev. Sci. Instrum.* **2002**, *73*, 2124−2127.
(23) Ravel, B.; Newville, M. *Phys. Scr.* **2005**, *T115*, 1007−1010.
(24) Rehr, J. J.; Mustre de Leon, J.; Zabinsky, S. I.; Albers, R. C. *J. Am. Chem. Soc.* **1991**, *113*, 5135.
(25) Nashner, M. S.; Frenkel, A. I.; Adler, D. L.; Shapley, J. R.; Nuzzo, R. G. *J. Am. Chem. Soc.* **1997**, *119*, 7760−7771.
(26) Mo, Y.; Antonio, M. R.; Scherson, D. A. *J. Phys. Chem. B* **2000**, *104*, 9777−9779.
(27) Benfield, R. *Chem. Soc. Faraday Trans.* **1992**, *88* (8), 1107−1110.
(28) Tolmachev, Y.; Timofeeva, E.; Hoover, R.; Frenkel, A. In *Proceedings of the 208th Conference of the Electrochemical Society*, Los Angeles, CA, Oct 16−21, 2005; The Electrochemical Society: Pennington, NJ, 2005; Abstract 1143.
(29) Kim, H.; Tremiliosi-Filho, G.; Haasch, R.; Moraes, I.; Wieckowski, A. *Surf. Sci. Lett.* **2001**, *474*, L203.